

Cellular Analysis Using Microfluidics

Michael G. Roper*

Department of Chemistry and Biochemistry, Florida State University, 95 Chieftain Way, Tallahassee, Florida 32306, United States

■ CONTENTS

Analysis of Intracellular Components within Living Cells	381
Noninvasive Methods for Examining Intracellular Components	381
Invasive Methods for Examining Intracellular Components	383
Secretion of Soluble Factors from Living Cells	385
Lysis of Cells for Measurement of Intracellular Components	387
Microfluidic Systems for Investigating Cellular Dynamics	389
Future Outlooks	392
Author Information	393
Corresponding Author	393
Notes	393
Biography	393
Acknowledgments	393
References	393

described, a brief discussion on the methods and/or findings is provided to showcase particular features of the developed system or to speculate how the method could be improved in future development.

■ ANALYSIS OF INTRACELLULAR COMPONENTS WITHIN LIVING CELLS

Most methods for analysis of intracellular components within living cells involve the use of a probe or sensor inserted through genetic or artificial means. While these methods have been utilized for decades, noninvasive methods are more ideal as there is less of a concern on how the probe changes the biological system. In this section, several examples of microfluidic-based devices using noninvasive and invasive measurement schemes for analysis of intracellular components are described.

Noninvasive Methods for Examining Intracellular Components. Although there are a number of methods for noninvasive measurement of the mechanical properties of cells,¹ this section is dedicated to measurement schemes that can provide noninvasive, intracellular measurements of a chemical nature. While noninvasive assays are ideal for reducing biological perturbations, the difficulties with these types of methods are a lack of specificity or sensitivity of the assays.

NMR is an example of a noninvasive method that is a powerful tool for identification but, due to its low sensitivity, is often impractical for obtaining information from small numbers of cells. To overcome this difficulty, in a 2015 paper, the Hergenröder group utilized a microfluidic system inside of an NMR sample holder for real-time detection of metabolites from tumor spheroids.² They designed an RF microslot probe based on planar electromagnetic waveguide technology and, using the microfluidic device, positioned the spheroid within the active area of the miniaturized probe. A nonmagnetic, on-board temperature sensor and heater controlled the temperature of the microfluidic system to maintain the viability of the cells for 24 h within the NMR instrument, enabling a time-resolved analysis of the metabolic profile of the spheroid.

The spheroid was composed of approximately 9000 cells from an HT29 human colorectal adenocarcinoma cell line. The microfluidic device was not a traditional planar system, but rather, a quartz glass capillary (length 30 mm, OD = 1.1 mm, ID = 1 mm) that had a Teflon filter at one end. In this way, when the capillary was held in a vertical position within the NMR sample holder, the spheroid rested at the bottom of the tube on top of the filter. Cell culture media was perfused into the top via diffusion from an external fluid reservoir. The end of

Cellular analysis is driven by the analytical methodologies available. Microfluidic systems that allow high throughput, single cell analysis, which used to be only a distant goal that researchers would strive for, are now commercially available. Because of the accessibility of this technology, it is now possible to perform quantitative and statistical analysis on unique systems and in novel ways. Much of the progress in this area stems from the ability of microfluidic devices to manipulate fluids with length scales comparable to the biology being investigated. The facile manipulation of micro- and nanoliter volumes is ideal for investigations of intra- and extracellular signaling from single cells or cellular populations. The purpose of this Review is to highlight and discuss novel papers, or fields of research, that were recently published and are expected to continue to develop in future years.

This article will focus on four main themes, each made possible through the use of microfluidic systems. These themes are analysis of intracellular components within living cells; the release of soluble components from living cells; lysis of cells for measurement of intracellular components; dynamic analysis of cellular systems. The Review will focus on selected articles published from the last two years (i.e., 2014–2015). Because there were several hundred articles published in this time frame relating to cellular analysis and microfluidics, this cannot be a comprehensive review. Instead, the articles highlighted here are meant to be representative of the general area of the aforementioned themes. An attempt was made to emphasize those manuscripts describing the development of novel analytical tools or assays, as opposed to the use of commercial systems or conventional detection strategies. After the paper is

Special Issue: Fundamental and Applied Reviews in Analytical Chemistry 2016

Published: November 30, 2015



the capillary containing the spheroid was centered on the $200 \times 100 \mu\text{m}$ microslot waveguide probehead (Figure 1). Using

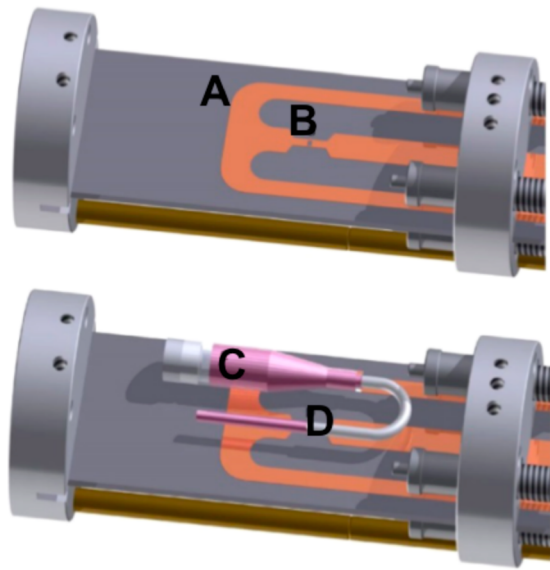


Figure 1. Coupling microfluidics to NMR. Shown is a schematic of the planar waveguide NMR probehead (A). The small slot in the copper strip (B) confines the magnetic field to the area of the microfluidic device (C) where the sample is located (D). Adapted from Kalfe, A.; Telfah, A.; Lambert, J.; Hergenröder, R. *Anal. Chem.* 2015, 87, 7402–7410 (ref 2). Copyright 2015 American Chemical Society.

simulations, they demonstrated that the B1 field distribution was confined to the slot in the microstrip detector where the spheroid was located. Proton NMR spectra were then acquired using a 600 MHz NMR spectrometer. To eliminate signal from macromolecules, a background correction was applied; to eliminate interference from water, the spectra were analyzed outside of where water was observed (4.5–5.5 ppm).

Results showed that most of the 23 metabolites that were being measured increased in concentration over 24 h, which they attributed to the increased biosynthesis of the fast growing tumor cells. They also detected a high rate of lactate accumulation indicating hypoxic conditions within the tumor spheroid. While still in its infancy, this method shows much promise. A more sophisticated microfluidic device would enable more complex biological experiments to be performed and longer-term monitoring. Notably, they state that the planar geometry of the probehead is amenable to more complicated devices, making it an attractive possibility for cellular analysis to a wide range of researchers. In the future, they aim to examine time-resolved metabolic response of cancer cells to targeted therapies.

Impedance spectroscopy is a powerful method for examining intracellular features in a noninvasive fashion.³ In this technique, an AC voltage is applied to the sample and the resulting current profile is measured as a function of applied AC frequency. Different cellular features will couple to the input waveform at particular frequencies. At low frequencies (<1 kHz), information on the extracellular microenvironment or cellular morphology can be discerned; midrange frequencies (<100 kHz) are used to detect the integrity of the cell membrane or cell wall; high frequencies (>500 kHz) can allow measurement of intracellular features.

In a 2014 paper, high-frequency contactless impedance spectroscopy was used to examine stress responses of human dermal fibroblasts.⁴ The microfluidic system was composed of a relatively simple channel design with four flow channels in parallel made in PDMS. Gold interdigitated electrodes were fabricated on glass and passivated with a 300 nm layer of silicon nitride (Si_3N_4) to eliminate ohmic and faradaic current while still facilitating cell adhesion. Impedance recordings over a large frequency range (500 Hz to 20 MHz) were recorded with the highest S/N found above 1 MHz.

The initial results from their sensors showed that responses were sensitive to changes in the cell density and cell damage in the microfluidic chamber. An innovative point of their work was the use of partial least-squares (PLS) regression of the time-resolved impedance spectra to improve the sensitivity of the system. PLS was used to help identify changes in the impedance spectra that were due to the biological system while minimizing noise, drift, and artifacts in the signal. Using PLS, the sensor response was observed to change when cells were stimulated with cycloheximide (a protein synthesis inhibitor), isoproterenol (stimulates β -adrenergic receptors activating ATP conversion to cyclic AMP (cAMP)), and serum starvation (lowers protein biosynthesis and decreases cell activity). While changes in the impedance spectra were observed as a result of these conditions, it is difficult to associate the signal changes with any particular biological change. A model of the system is often necessary to correlate the signal change to the underlying physical phenomena.

This strategy of using a model in conjunction with the impedance data was employed in a paper published in 2014 where a single cell impedance method was used in conjunction with a finite element model (FEM) to detect underlying subcellular differences in yeast cells.⁵ With this integrated system, they were able to discriminate between wild-type and mutant yeast cells, which differed in size and distribution of vacuoles in the intracellular fluid. The wild-type (B4741) strain had 1–4 normal-sized vacuoles, whereas the B4741 vac8Δ::KanMX strain contained 2–10 small vacuoles.

The novel feature of their report was the use of extremely high AC frequencies, up to 500 MHz. As mentioned before, the use of such large frequencies allows intracellular organelles to contribute to the observed response. Beyond 50 MHz, discrimination of the two yeast strains became possible because of the larger vacuoles in the wild-type cells.

The microfluidic channel design was simple, consisting of two glass pieces with two pairs of planar Pt electrodes patterned on the top and bottom glass plates adjacent to the channel. Both wild-type and mutant cell types were flowed together through the device with 4 μm diameter polystyrene beads. To compensate for cell size and position between measurement electrodes, an “opacity” was calculated which normalized the impedance values of the cells at all frequencies to the impedance found at 0.5 MHz. When the applied frequency was above 50 MHz, the two cell types could be differentiated on the basis of their opacity spectra. The difference in the spectra was attributed to the larger vacuoles in the wild-type cells, which contain high concentrations of charged proteins.

To obtain quantitative values of cellular dielectric properties, the data were further reduced to a “relative opacity” by normalizing the opacity of the cells to the opacity of the 4 μm diameter polystyrene beads. This second normalization compensated for measurement electronics and other nonidealities in the system. These relative opacities were compared

to results from a FEM of the microfluidic channel containing a “wild-type” and “mutant” cell where the wild-type model cell contained a single vacuole and the mutant cell contained none. A good agreement between measured and simulated relative opacity values were observed for frequencies from 0.5 to 100 MHz. Using this model, they were able to extract quantitative information about the dielectric properties of the conductivity and permittivity of the cell wall, cell membrane, cytosol, vacuole membrane, and vacuole.

Impedemetric sensing is a growing method used for noninvasive sensing of cellular systems. There are still questions of the measurement specificity, but it is likely that with continued development of both the instrumentation and modeling, these questions can be answered. Due to the straightforward nature of its measurement scheme and its ability to peer into the intracellular milieu, this noninvasive method should be simple to integrate into other microfluidic systems for increasing the information content of the cellular system being investigated.

Invasive Methods for Examining Intracellular Components. Within ~10 years of the first reports describing microfluidic systems, they were being used to analyze intracellular components.^{6–8} In this section, several reports that have been published in the last two years are supplied that focus on the development of novel analytical methods or novel uses of microfluidic systems.

While enzymes are involved in all major cellular processes, our understanding of their thermodynamic and kinetic properties is limited due to the traditional method of measuring these parameters *ex vivo*. Instead, methods that can measure enzyme kinetics *in situ* would allow more biologically relevant insights due to crowding effects, local concentration gradients, and perhaps unforeseen regulators.

A paper published in 2015 described a microfluidic system for measurement of the intracellular activity of alkaline phosphatase (AP), an essential enzyme in many intracellular processes such as metabolism and genetic transduction, as a function of temperature.⁹ Previously, a multifunctional microfluidic pipet was developed that could be held in a traditional micromanipulator and used to deliver small volumes of solution to a defined location outside the tip of the device.¹⁰ In the most recent report, they updated the design so that four solutions could be delivered to an $\sim 90 \times 80 \mu\text{m}$ area, enabling stimulation of single adherent cells (Figure 2A). They used this system in conjunction with localized heating by an IR diode laser to determine the effect of temperature on the activity of intracellular AP.

The experimental protocol consisted of applying four different solutions to a single cell using the microfluidic pipet. First, α -hemolysin was applied to form pores in the cell membrane; buffer was then applied to wash the mildly permeabilized cells, and finally, the nonfluorescent substrate of AP, fluorescein diphosphate (FDP), was applied. During application of the substrate, the IR laser was used to hold the temperature constant allowing FDP to enter the cell and be cleaved to its fluorescent product, fluorescein, by AP. Five sequential temperatures were tested, 22, 27, 32, 37, and 42 °C, each held for ~40 s. The temperature surrounding the cell was controlled by modulating the applied current at the IR laser source. Finally, the health of the cell membrane was tested by using the microfluidic pipet to deliver a solution of fluorescein and making sure that it was not taken up by the cell.

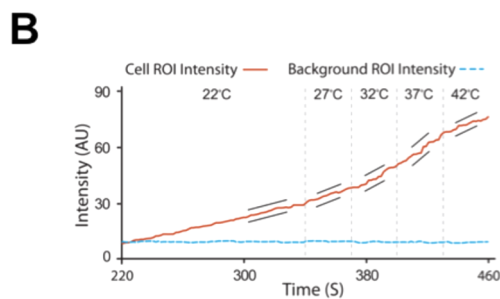
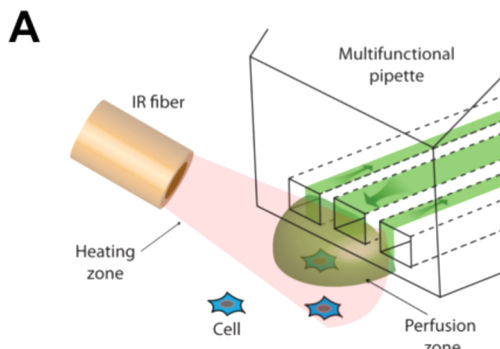


Figure 2. Measurement of *in situ* enzyme kinetics. (A) An artistic view of the end of the multifunctional pipet situated close to a single cell. Solution is expelled from the device in a small region confining the stimulation to a single cell. Simultaneously, an optical fiber coupled to an IR laser is used to control the temperature of the selected region. (B) Shown in red is the raw data of fluorescence accumulation within a single cell at different temperatures, used to compute the effect of temperature on AP activity. The black lines show the average rate of change of the fluorescence data at the various temperatures, while the blue line indicates the intensity of the background. Adapted from Xu, S.; Ainla, A.; Jardemark, K.; Jesorka, A.; Jeffries, G. D. M. *Anal. Chem.* 2015, 87, 381–387 (ref 9). Copyright 2015 American Chemical Society.

AP activity in each cell was extracted from the slope of fluorescence vs time at each temperature point (Figure 2B) and was then normalized to the value observed at 37 °C. These enzymatic efficiencies showed an increase as a function of temperature, obtaining a maximum at 37 °C, and then a slight drop in efficiency at 42 °C. The authors did not compare *in situ* vs *ex vivo* measured enzymatic efficiencies, but did observe a change in the distribution of efficiencies in HEK cells at the highest temperature tested (42 °C). This was in contrast to what was seen in NG cells, and the authors speculated that this may indicate that something within the NG cells allows the structure of AP to be better stabilized at elevated temperatures.

To confirm their methodology, the efficiency of a second enzyme, protease, was also examined using casein BODIPY FL as substrate. Again, the highest efficiency was observed at physiological temperatures. Several control experiments were performed to ensure the measured results were accurate; for example, they demonstrated that the permeabilization of the cells was not temperature dependent, the emission intensity of fluorescein was not temperature dependent, and the thermal stability of AP was also investigated. While this is one of the few techniques available for measuring intracellular enzymatic activities without requiring lysis of the cell or extraction of the enzyme, the measurement scheme hinges on the availability of substrates that are specific and have a spectral (or other type of) shift upon conversion. Also, with continued technological

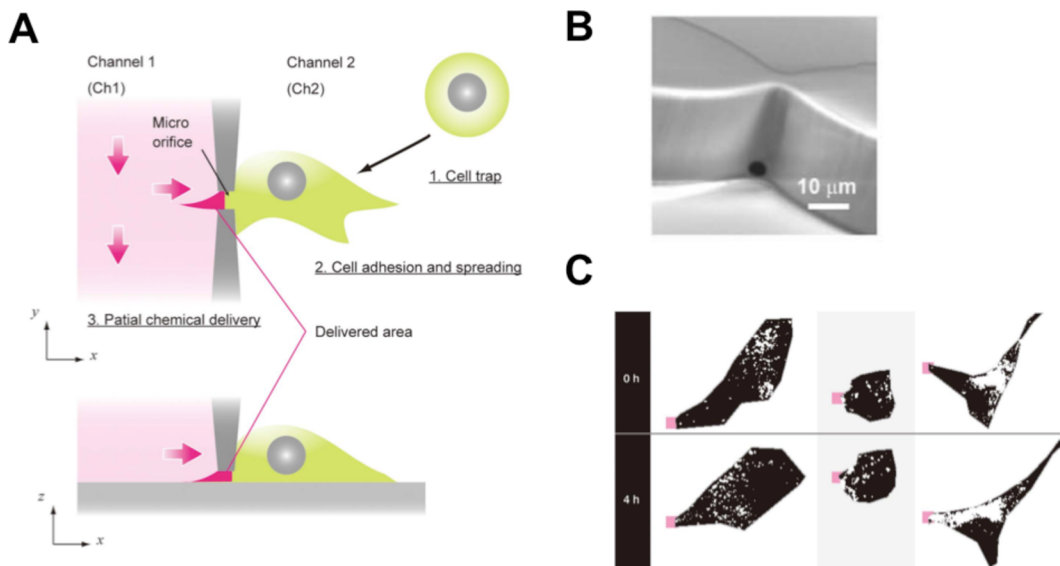


Figure 3. Subcellular microfluidic stimulation. (A) A schematic view of the cell trapping (top) and stimulation (bottom) are shown. Due to a pressure differential between the two channels, a cell is drawn toward the orifice where it blocks this opening. Application of a stimulant to the left channel then spatially confines the delivery of the stimulant to the area around the orifice. (B) A magnified view of the circular orifice is shown. (C) Three MIN6m9-C4 cells are shown where the GFP-labeled insulin granules are seen as white dots. The location of the orifice is indicated by the pink box. The top row of images shows the granule locations prior to stimulation, and the bottom row after 4 h of stimulation with 25 mM glucose. In all cases, the position of the center of mass of the granules has shifted in the direction of the orifice where the glucose level was high. Adapted from Terao, K.; Gel, M.; Okonogi, A.; Fuke, A.; Okitsu, T.; Tada, T.; Suzuki, T.; Nagamatsu, S.; Washizu, M.; Kotera, H. *Sci. Rep.* 2014, 4, 4123 (ref 11), with permission from Nature Publishing Group.

refinements, the throughput of this system could be improved so that multiple cells may be interrogated at the same time.

In a paper published in 2014, a microfluidic device was used to spatially confine delivery of glucose to subcellular localizations on single pancreatic β -cells.¹¹ These cells are found in pancreatic islets of Langerhans and secrete the hormone insulin in response to glucose. Within islets there are several other cell types, each responsible for releasing different peptides to help regulate glucose levels. A spatial organization exists among these various cells with respect to the blood vessels that permeate the intraislet space. There is even subcellular organization within the β -cells so that the intracellular insulin granules are polarized closer to the side of the cell facing the venous capillary. How this subcellular distribution is formed and by what factors is still unknown.

To investigate how β -cells polarize, a PDMS microfluidic device was developed that had two flow channels separated by a solid wall. Within the wall, there was an orifice, smaller than a cell, connecting the two channels. Cells were delivered to one of the channels (e.g., channel 2) where it would become trapped at the micro-orifice due to the pressure differential between the channels (Figure 3A). The trapped cell was then allowed to adhere and spread across the orifice, sealing it. Chemical substances were then introduced into the other channel (e.g., channel 1), which resulted in delivery of the substances to only the part of the cell that was at the orifice. The area of the cell surface stimulated was estimated to be $104 \pm 54 \mu\text{m}^2$ ($\sim 11\%$ of the total cell surface).

The fabrication of the orifice within the device was described in a previous report.¹² First, an SU-8 mold of the channels was made on a Si substrate. Then, an acrylic polymer solution was coated onto the mold and dried. When it dries, a “meniscus bridge” forms at the narrowest gaps between the SU-8 structures. These bridges have a circular shape to their cross

section, and when PDMS is poured onto the mold and cured, the circular orifice is produced (Figure 3B). By controlling the percentage of the acrylic polymer solution and the distance of the SU-8 structures, the size and locations of the orifices can be tuned, respectively.

The authors also developed a clonal cell line containing GFP-labeled insulin, termed MIN6m9-C4. Using confocal microscopy, individual vesicles containing the GFP-labeled insulin could be observed in single cells. The MIN6m9-C4 cells were introduced into channel 2 and allowed to seal the orifice. Different glucose concentrations were then applied to channels 1 and 2 to introduce localized stimulation of the cells. After 4 h of 25 mM glucose applied to channel 1 and 0 mM glucose to channel 2, a shift in the vesicles to the high glucose side was observed (Figure 3C). The shift toward the high glucose side was approximately $5 \mu\text{m}$, which was a significantly greater shift than control experiments that used 0 and 0 mM or 25 and 25 mM glucose in channels 1 and 2, respectively.

The benefit of this device was the simplicity in the fabrication and the potential uses of the methodology. One could envision this method as a means for performing patch clamping simultaneously on a large number of cells. Currently, they were examining only one or two cells at a time, but they have the potential to array these orifices in large numbers on a single chip. In their current design, they also have no dynamic information from the cells, taking only two fluorescent images, one at the beginning of the experiment and one at the end. They can likely improve their imaging capabilities to enable imaging the vesicles over the course of the experiment. Nevertheless, the authors believe that adapting the device to cell polarity studies will accelerate the *in vitro* understanding of how intracellular heterogeneities are induced by the chemical environment.

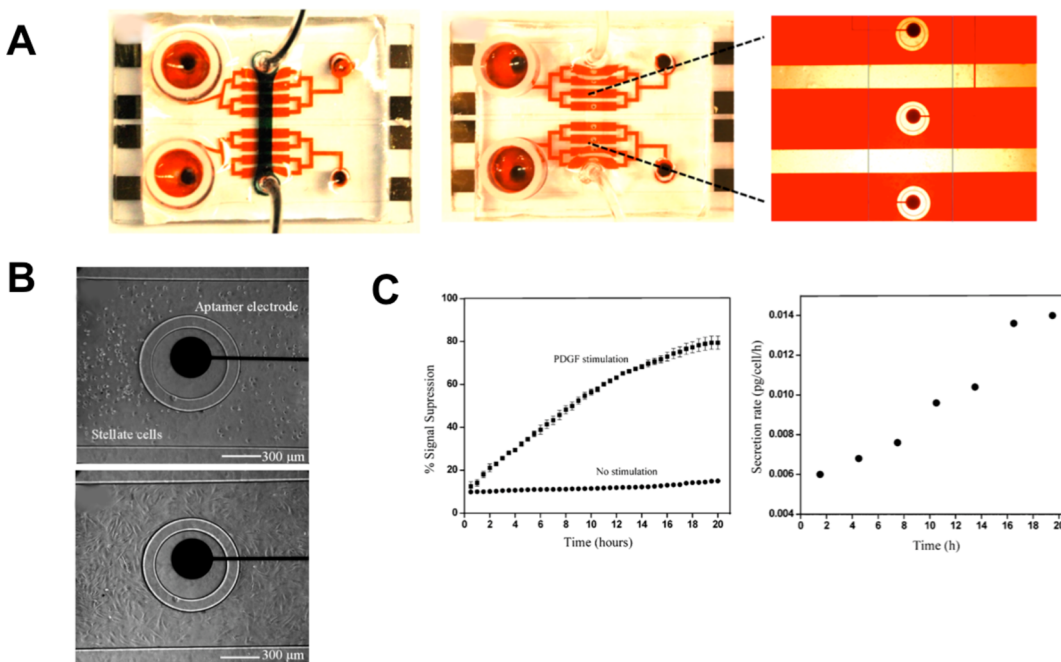


Figure 4. Aptasensor integrated into a reconfigurable microfluidic device. (A) The microfluidic device is shown where the fluid and control channels are filled with red and black dye, respectively. The image on the left shows the device with the microcups raised, and the middle and right images show the microcups lowered over the electrodes. (B) Photograph of the initial seeding of hepatic stellate cells into the channel (top) and after 12 h (bottom). Note the absence of cells near the electrode due to the protection of the microcup. (C) The cumulative release of TGF- β 1, measured as the % of MB signal suppression, following PDGF and control stimulation (left). The secretion rate (right) was found using the cumulative signal and a numerical model for production, diffusion, convection, and binding of TGF- β 1 to the aptasensor. Adapted from Matharu, Z.; Patel, D.; Gao, Y.; Haque, A.; Zhou, Q.; Revzin, A. *Anal. Chem.* 2014, 86, 8865–8872 (ref 13). Copyright 2014 American Chemical Society.

■ SECRETION OF SOLUBLE FACTORS FROM LIVING CELLS

Cellular communication is enabled through the release of soluble factors. The analysis of the released components is a difficult endeavor due to the multitude of factors that can be released, the dynamic nature of the secretion (changing concentration in time), and the often incompatibility of cellular culture conditions with analytical detection methodologies. The following papers highlight novel methods or techniques applied to this important field of research.

The liver is the epicenter of metabolism, and its dysfunction is a main cause of several diseases. Liver fibrosis is an inflammatory condition present during liver injury, cancer, or infection. TGF- β 1 is a secreted factor by hepatic stellate cells and is associated with fibrosis of liver and other organs. TGF- β 1 is known to cause the irregular production of ECM proteins resulting in a loss of the differentiated hepatic phenotype in stellate cells. It is therefore important to measure the dynamics of its release over the course of injury or insult.

In a 2014 paper, the Revzin group continued their development of reconfigurable microfluidic devices coupled with aptasensors for the measurement of TGF- β 1 release from hepatic stellate cells.¹³ The microfluidic device consisted of two PDMS layers on a glass slide with micropatterned Au electrodes. The Au electrodes were fabricated by photolithography in arrays of eight electrodes with 300 μ M diameters. One PDMS layer was used as the control layer for actuation of the working microfluidic layer (Figure 4A, left two images). The working layer had 8 channels with each channel having 4 microcups, with inner and outer diameters of 500 and 700 μ m, respectively, and a height of 60 μ m. Application of pressure to the control layer brought the microcups over the

electrodes isolating them from the extracellular environment (Figure 4A, right image).

The electrodes were coated with phosphorothioate-modified TGF- β 1 aptamers through 3' thiol linkages. The 5' end of the aptamer was covalently linked to methylene blue (MB). Square wave voltammetry (SWV) was performed from 0 to -0.50 V at a frequency of 60 Hz for measurement of MB. As the aptamer binds TGF- β 1, a change in conformation of the aptamer moves MB away from the electrode surface, reducing the measured current. Using surface plasmon resonance, they found the optimum aptamer concentration to be 1 μ M for target binding while the K_d was determined to be 1 nM. The specificity of the aptasensor to nonspecific proteins was less than 10% of the signal generated for TGF- β 1. Finally, other isoforms of TGF- β were tested, and they observed approximately 15% and 30% cross-reactivity for the β 2 and β 3 isoforms, respectively. The range of the biosensors was 1–250 ng mL⁻¹ with a LOD of 1 ng mL⁻¹.

To load the cells in the device, the cups were lowered, protecting the electrodes, and stellate cells were immobilized within the working channels (Figure 4B). After a predetermined incubation time, the cups were raised and the cells were stimulated by infusion of 20 ng mL⁻¹ platelet-derived growth factor (PDGF) while the release of TGF- β 1 was monitored over 20 h (Figure 4C). Four of the microchannels were used to measure TGF- β 1 release from cells, while the other four measured release from nontreated cells. To analyze the results, a numerical model for production, diffusion, convection, and binding of TGF- β 1 to the aptasensor was used, by assuming a constant secretion rate in each 3 h time interval. From the modeling results, the average TGF- β 1 release rate for PDGF-

stimulated cells was $0.0140 \text{ pg cell}^{-1} \text{ h}^{-1}$ while for control cells it was $0.0009 \text{ pg cell}^{-1} \text{ h}^{-1}$ (Figure 4C).

The values of TGF- $\beta 1$ release were higher than what others have reported, which the authors said may be explained by enhanced sensitivity of their microfluidic approach. Given the importance of TGF- $\beta 1$ signaling in a range of diseases, the ability to monitor release of TGF- $\beta 1$ has high significance. An exciting feature of this system is that the approach is relatively general and could be used to monitor cellular release from other cells assuming the appropriate aptamer is available. They have also demonstrated the ability to multiplex the aptasensor detection method, for increased information content.¹⁴ Time-resolved measurements would be an important feature to incorporate, so that the assumption of a constant secretion rate would not have to be made. There are published methods on the regeneration of aptamer sensors,¹⁵ and the Revzin group has published a method using a denaturing buffer in combination with the microcups.¹⁶

Adipocytes were once thought of as only the fat storage cells of the body, yet recently, the endocrine properties of these cells have begun to be appreciated. Besides a number of proteins released from these cells, they also secrete glycerol and nonesterified fatty acids (NEFA) as result of the lipolysis of triglycerides. Increased adiposity is often associated with a number of metabolic disorders; therefore, understanding the dynamics of factors released from these cells will allow a better understanding of the role that these cells play in a number of diseases associated with obesity. What complicates the measurement of NEFA release is that the cells can reuptake and re-esterify the secreted NEFA back into triglycerides. Since glycerol is not recycled in the same way, a simultaneous measurement of NEFA with glycerol helps in the accounting of secreted and re-esterified NEFA.

The Kennedy group has developed several microfluidic devices for the online monitoring of cellular release from adipocytes.^{17–19} In a 2014 paper, they used a 4-layer PDMS microfluidic device for culture and perfusion of 3T3 adipocytes with an on-chip dual-enzyme assay for real-time measurement of both NEFA and glycerol secretion.²⁰ Preadipocytes were first cultured on coverslips and differentiated into adipocytes using conventional methods. Finally, the multilayer microfluidic device was enclosed around the adipocyte-coated coverslip, integrating a perfusion system and a channel network for measurement of NEFA and glycerol release (Figure 5A).

The chip was designed such that the cellular perfusate split evenly into two channels for separate measurement of the two analytes. The portion of the perfusate used for measurement of glycerol mixed with two solutions. One contained the fluorogenic dye, Amplex UltraRed, and the other contained the glycerol reagents, which contained ATP, glycerol kinase, and glycerol phosphate oxidase. The portion of the perfusate used for measurement of NEFA mixed with three solutions. First, it mixed with "Color Reagent A", then Amplex UltraRed, and finally with "Color Reagent B". Since these were commercial kits, there was no mention of the exact ingredients of the color reagents; however, the authors did state that they contained coenzyme A (CoA), ATP, acyl-CoA synthetase, and acyl-CoA oxidase. The result of both assays was the production of H_2O_2 , which then reacted with peroxidase and Amplex UltraRed to create the detected fluorescent product. The detection points of both assays were in close proximity to one another, allowing simultaneous measurement with a CCD camera. Because of the multiple inlets for the various reagents

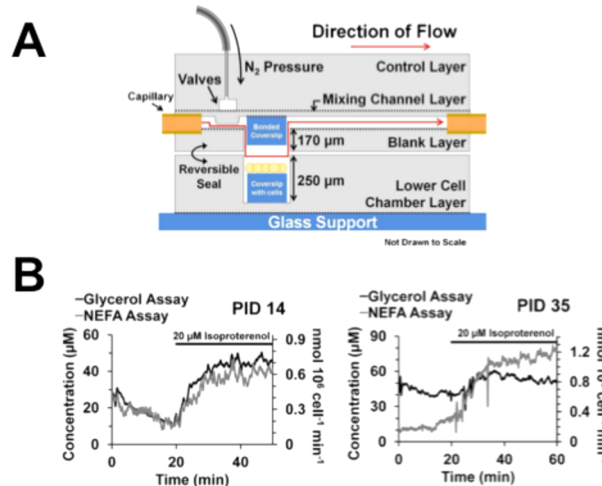


Figure 5. Multilayer microfluidic device for measurement of NEFA and glycerol release. (A) Side view of the multilayer PDMS device used for stimulating adipocytes. Adipocytes were cultured on glass coverslips and placed into the bottom layer of the microfluidic device. The fluidic channels used for the NEFA and glycerol assays were in the next layers, while the valve control channels were in the upper layer. (B) The release of glycerol (black line) and NEFA (gray line) from two experiments showing different ratios of NEFA/glycerol secreted as a function of time. Adapted with permission from Springer Science +Business Media: *Anal. Bioanal. Chem.*, Multiplexed microfluidic enzyme assays for simultaneous detection of lipolysis products from adipocytes, Vol. 406, 2014, pp. 4851–4859, Dugan, C. E.; Cawthorn, W. P.; MacDougald, O. A.; Kennedy, R. T. (ref 20), Figures 2 and 7A,B, Copyright Springer-Verlag Berlin Heidelberg 2014.

that were required for each assay (three for NEFA and two for glycerol), care had to be taken in choosing the flow rates to ensure the flow would proceed through the channel design as intended, with good assay sensitivities and fast response times. A FEM was used to help design the device to achieve this goal.

PDMS was chosen as the substrate since it allowed integration of valves and other features. However, they found that surface modification with SDS was necessary to prevent NEFA from adsorbing to the device. With this system, the glycerol assay had a LOD of $5 \mu\text{M}$ and was linear through $110 \mu\text{M}$, while the NEFA assay had a LOD of $6 \mu\text{M}$ and was linear through $150 \mu\text{M}$. Their prior work used manual connections for delivering reagents to the cells, which required both starting and stopping flow rates during the course of the experiments. This starting and stopping caused changes in pressure on the devices, which affected the detected signal. They found this to be especially problematic with the dual-channel chip with multiple flow paths. To remedy this problem, they incorporated integrated valves into their device, which significantly improved the stability of the flow creating smooth changes in reagent concentrations as well as reduced dead volumes and increased the automation of the device.

Using the system, they found that basal concentrations of both NEFA and glycerol were above the LOD for all cases. To initiate lipolysis, isoproterenol was added and produced a simultaneous increase in both analytes. As mentioned before, the simultaneous measurement of NEFA and glycerol allows an assessment of NEFA recycling. In one set of experiments, the authors observed a NEFA/glycerol ratio of 1:1 before and after stimulation with isoproterenol, implying the recycling did not change after stimulation (Figure 5B). In another set, they saw a NEFA/glycerol ratio of 1:3 that changed to 2:1 when

challenged with isoproterenol (Figure 5B), suggesting high recycling that decreased with stimulation. Finally, they examined the effect of the age of adipocytes (postinduction) on the NEFA/glycerol ratios and found that while the basal ratios decreased with age, after stimulation, the ratio increased for the more mature adipocytes. The authors stated that the cause and significance of these trends were not known, but may be due to the resulting lipid content in the cells as they aged in culture.

An exciting feature of this report was the incorporation of commercial-based enzymatic assays into a microfluidic system and obtaining near real-time monitoring of cellular release. One could envision a number of commercially available enzymatic assays being used for quantitation of various analytes of interest. As the authors showed, some optimization of the channel design would be required to ensure appropriate sampling of the perfusate by the various assays, but could lead to a powerful, multiplexed system.

■ LYSIS OF CELLS FOR MEASUREMENT OF INTRACELLULAR COMPONENTS

Microfluidic devices are ideal platforms for sample preparation,^{21–23} and this is especially true for cellular systems.²⁴ The volume compatibility of microfluidic systems and cellular architectures means small dilution factors which enables highly sensitive measurements. Recent examples of microfluidic devices used for analysis of intracellular components are described below.

The Herr group continues to build on their single cell Western blotting (*scWestern*) technique. The *scWestern* method supports the parallel analysis of thousands of simultaneous single-cell Western blots, each composed of chemical lysis, protein electrophoresis, UV-initiated blotting, and in-gel probing with fluorescently labeled antibodies.²⁵ The ability to probe such a large number of single cells simultaneously is ideal for identifying cell-to-cell variations as well as the response of the ensemble. In a paper published in 2014, they described a method that allowed whole-cell fluorescence imaging prior to the *scWestern*, with the ability to archive samples on the gel for future analysis.²⁶

The fluorescence imaging allowed phenotypic assessment of live cells, which was then correlated with protein expression analyses to characterize cell-to-cell variation in drug response in a cultured model of human glioblastoma multiforme. The authors stressed the importance of phenotype-to-proteotype characterizations due to the finding that fewer than 50% of protein changes correlate with mRNA changes.²⁷ The *scWestern* imaging platform provides high-specificity protein measurements with single-cell phenotype resolution.

The microfluidic device used an array of microwells made in a 30 μm layer of photoactive polyacrylamide gel on a glass microscope slide. The diameters of the wells (32 μm) were chosen so that the majority had only one cell. Cells were gravity-settled onto the slide, and the cells were imaged by both phase contrast and fluorescence imaging. Phenotype imaging consisted of phase contrast, DNA staining for cell identification, daunomycin (DNR) imaging to assess drug uptake, and Annexin V to assess cell viability (Figure 6A).

After imaging, cells were chemically lysed by pouring a lysis buffer over the slide. The lysis procedure was optimized to minimize protein loss from the shallow microwells. The optimum procedure used a lid to enclose the microwells to reduce diffusional losses, and lysis occurred within 20 s.

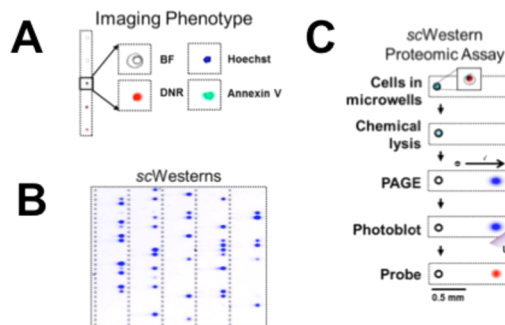


Figure 6. Protocol for integration of whole-cell fluorescence imaging prior to single cell Western blots. (A) Cells loaded into an array of microwells were imaged for phenotypic assessment using a combination of phase contrast and fluorescence microscopy. (B) Cells were then lysed, and the lysate was analyzed by gel electrophoresis. (C) The separated proteins were then immobilized into the gel and blotted using fluorescently labeled antibodies. Adapted from Kang, C.-C.; Lin, J.-M. G.; Xu, Z.; Kumar, S.; Herr, A. E. *Anal. Chem.* 2014, 86, 10429–10436 (ref 26). Copyright 2014 American Chemical Society.

Immediately after, an electric field (40 V cm^{-1}) was applied across the device drawing the intracellular content from the wells into the surrounding polyacrylamide gel for separation (Figure 6B). The separation length was 1 mm, determined by the distance between the microwells. They also optimized the polyacrylamide gel formulation for separation of the size range expected. Separated proteins were then immobilized, via UV activation, to benzophenone residues cross-linked into the gel. The proteins were then probed by fluorescently labeled antibodies and scanned by a fluorescence microarray scanner (Figure 6C).

Using this device, they assessed the apoptotic response to DNR treatment of U373 cells by Annexin V staining and by *scWestern* blotting for GAPDH (internal control) and cleaved caspase 8, an apoptosis marker. They observed a positive correlation, confirming a strong association between phenotype and protein expression at a single-cell level. The false positive rate (imaging showed no staining, whereas the blotting showed cleaved caspase 8) was less than 1%, and they attributed that to the potential diffusional cross-talk between occupied wells and neighboring empty wells. The false negative rate (imaging showed staining, but nothing was detected on the gel) was higher at ~30%, which was attributed to diffusional losses of material from the occupied wells.

They also found that DNR uptake did not positively correlate with cell apoptosis. One possible mechanism for this result was the presence of active efflux of the drug through multidrug resistance proteins, such as P-glycoprotein (P-gp). They found that, although higher amounts of P-gp were detected in DNR-treated U373 cells as compared to control cells, there was no statistical correlation between P-gp expression and drug uptake. They concluded that P-gp was not a major contributor to drug uptake or drug resistance under these conditions. This result also allowed them to evaluate the ability of their devices for long-term storage as new biological hypotheses evolved. They demonstrated that, after 4 months of storage at room temperature, 83% of the signal from a fluorescently labeled antibody was still present and they could strip stains from a gel that had been stored for 7 months. These results suggested that these devices are feasible for long-term archival storage.

The scWestern method is powerful in its ability to perform high throughput measurements with a relatively simple microfluidic architecture. A factor that was limiting in this report was the high false negative rate, but it is likely that, with increased design iterations, this value could be decreased.

Due to their ubiquity, there is a large interest in measuring cellular kinase activity levels. Kinases catalyze the phosphorylation of specific substrates within the cell, and it has been proposed that variability in protein activity may lead to a different response to drugs. In a paper published in 2014, a microfluidic device was developed for measuring kinase activity from single cells.²⁸

The PDMS microfluidic chip was composed of 5 parallel sample channels that combined to a single outlet. Gravitational flow was used to drive solution from the inlets to the outlet. To concentrate the samples within these channels, a Nafion membrane was fabricated between the sample channels and a buffer channel running in parallel using a microflow patterning technique.^{29,30} Application of a low voltage from the sample to the buffer channel across the junction allowed migration of the cations out of the sample channel into the buffer channel, but did not allow anions to pass, creating an ion depletion zone near the membrane. The conductivity gradient at the boundary of the ion depletion zone produced a stable electric field gradient that focused negatively charged biomolecules at separate locations in the sample channel where their electrophoretic velocities balanced the bulk flow velocity. This type of design has been shown to induce a million-fold concentration enhancement.³¹

Fluorescently labeled peptides containing recognition sequences for specific kinases were used as substrates. Kinases in the sample that recognized these peptides would then phosphorylate them, leading to an increase in electrophoretic mobility. Two bands were therefore observed, corresponding to phosphorylated and nonphosphorylated fluorescent peptides. The average kinase reaction rate was directly calculated from the fraction of phosphorylated substrate observed. Importantly, because the assay is ratiometric, the positions of the bands, which are sensitive to several experimental factors, does not affect the calculation of this fraction.

Limits of detection of recombinant Akt, MK2, and PKA were 1, 1.2, and 0.7 ng/mL, respectively. They used their method for assaying the fraction of Akt and PKA substrates phosphorylated from bulk HepG2 cell cultures and observed higher fractions of phosphorylated substrates under insulin- or forskolin-stimulated conditions compared to serum-starved conditions. These initial bulk cell assays demonstrated that the sensitivity of their assays could be applied to single cell measurements.

Single cell assays were performed by allowing cells to settle onto an array of 40 nL microwells. After an overnight incubation, the cells were washed, and a solution containing fluorescently labeled peptides, phosphatase and protease inhibitors, and inhibitors of off-target kinases was added. Finally, the wells were capped with tape and the device was placed in an ultrasonic water bath for 30 s for cell lysis. The lysate was then allowed to react with the substrates for 90 min prior to stopping the reaction by diluting the solution to 12 μ L. The initial low volumes used for the reaction were to contain the kinases in a small volume to prevent dilution and allow a substantial fraction of the fluorescent peptide to be phosphorylated. Ten μ L of this solution was then analyzed in their microfluidic device. Even after such a large dilution, the

concentrating effect of their device enabled observation of the phosphorylated peptides.

The difficulty of multiplexing the kinases assayed in a single run is that a staircase-like electric field profile is required. This is because the analytes will focus at the high electric field gradients, but the plateaus are required for spatial resolution of the different components. To achieve this profile, they added intermediate mobility spacers that became so concentrated that they altered the E-field. Interestingly, they used custom synthetic peptides as the spacers because they could control the mobility of these species based on their sequence. They developed a series of peptides that had mobilities between substrates and phosphorylated products and demonstrated simultaneous concentration and resolution of substrates and products corresponding to PKA, Akt, and MK2.

This is a fairly simple, yet powerful, microfluidic device for concentrating low amounts of material. It is unclear what peak capacities can be produced with this system, but they do caution that use of an increased number of spacer peptides would lead to a reduced concentration of the analytes. This is due to having multiple steps in the E-field staircase, and as a result, the gradient is reduced. They also found that, at high-applied voltages needed for multiplexing, the bands in the current device were not stable over extended amounts of assay time needed to achieve single cell detection sensitivity. The authors stated that more device and material optimization was needed to perform simultaneous activity assay for three or more different kinases from single cells. Nevertheless, with continued optimization and integration with sample preparation steps, this method should allow one to have the ability to study the functional relationship between kinases yielding insights on the inner-workings of cell regulatory pathways.

Microfluidics has enabled multiple tools that can be used for single cell genetic or transcriptomic measurements, and single cell proteomic methods are even becoming more popular,^{32,33} however, quantitative single cell metabolic assays have proven more challenging. One of the challenges is that there are multiple classes of metabolites, which often require multiple measurement formats.

In a 2015 paper, the Heath group developed a microfluidic-based method for quantitative analysis of proteins and metabolites from single cells.³⁴ They used this device to investigate connections between protein signaling networks implicated in tumor metabolism and growth and the small molecule metabolites that provide energy sources. This device therefore provides a connection between two important classes of oncology biomarkers.

In previous work, this group developed methods for barcoding quantitative measurements of proteins using calibrated immunofluorescence assays, similar to conventional sandwich assays.^{35,36} They have used this technique for measurement of proteins from single cells using a single cell barcode chip (SCBC). In this work, they integrated the measurement of four metabolites (cAMP, cyclic GMP (cGMP), glutathione (GSH), and glucose) with the SCBC (Figure 7A).

The SCBC consisted of 310, 1.5 nL microchambers where each chamber contained antibody-coated stripes specific for different intracellular proteins. The stripes were produced using a DNA-encoded antibody library (DEAL) approach that they had previously developed.³⁷ For measurement of cAMP, cGMP, and GSH, commercially available antibodies were available, which enabled the production of similar types of barcoded sites within each microchamber for these metabolites;

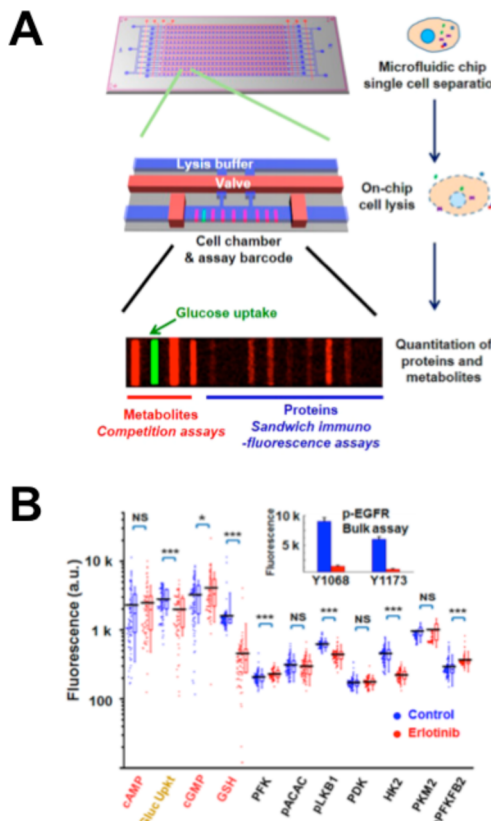


Figure 7. Single cell barcode chip integrating both metabolite and protein assays. (A) A single cell barcode chip is shown (top) where cells are loaded into individual wells, followed by delivery of lysis buffer using on-chip valves (middle). The intracellular proteins and metabolites then diffuse to the barcoded assay site where competitive and sandwich assays are performed for metabolites and proteins, respectively (bottom). (B) Data from barcode experiments where intracellular metabolites and proteins from single cells from a GBM39 neurosphere tumor model were interrogated. The metabolite levels are shown in the first 4 columns and intracellular proteins in the next 7 columns. Each data point represents the results from a single cell, with the average represented by the horizontal black bar. Levels of metabolites and proteins from cells incubated with erlotinib are shown in red and control cells in blue. The inset shows the results from a bulk assay for phosphorylation sites on epidermal growth factor receptor (EGFR) and indicates that erlotinib inhibited phosphorylation. Adapted from Xue, M.; Wei, W.; Su, Y.; Kim, J.; Shin, Y. S.; Mai, W. X.; Nathanson, D. A.; Heath, J. R. *J. Am. Chem. Soc.* 2015, 137, 4066–4069 (ref 34). Copyright 2015 American Chemical Society.

however, pairs of antibodies, necessary for sandwich assays, were not available. Thus, competitive-based assays were developed using a fluorescently labeled variant of GSH and horseradish peroxidase (HRP)-labeled cAMP and cGMP. During lysis of the cells, known amounts of these labeled competitors were added to the lysis buffer to compete with the native metabolites for binding to the antibodies. Measurement of the labeled GSH, cAMP, and cGMP bound to the antibodies was then indirectly correlated to the amount of native analytes. These assays had an added benefit in that the expected intracellular concentrations of GSH (mM level) were readily detectable, whereas lower intracellular levels of cAMP and cGMP were amplified using HRP.

In contrast to these other metabolites, no suitable method for glucose could be readily incorporated into their SCBC device. To overcome this, an assay was developed using a glucose-

biotin conjugate (Gluc-Bio), which the authors showed was actively taken up by the cells and used as a substrate by hexokinase, in a similar manner as 18F-fluorodeoxyglucose. After cell lysis, the Gluc-Bio that was taken up by the cells competed with native glucose for binding to Alexa-Fluor 555-labeled streptavidin that had been immobilized in the microchambers. Biotin-BHQ2 was then added which bound to any unoccupied sites, quenching the streptavidin fluorescence. In this way, the fluorescence intensity of the streptavidin barcode site correlated with the amount of Gluc-Bio taken up by the cell. The authors stated that the assays for GSH, cAMP, and cGMP were quantitative, but the assay for glucose was only useful for relative quantitation.

Their experiments consisted of examining seven metabolism-related proteins and phosphoproteins, in addition to the metabolites mentioned above, from cells taken from a GBM39 neurosphere tumor model following 24 h of erlotinib treatment. Erlotinib is a tyrosine kinase inhibitor, acting on the epidermal growth factor receptor (EGFR). A typical set of data from an SCBC device yields ~100 single-cell assays and ~100 0-cell assays for background signal levels. Using their device, they confirmed that erlotinib significantly inhibited EGFR phosphorylation and suppressed glucose uptake and hexokinase activity (Figure 7B). They also found strong correlations between cAMP and cGMP, between glucose uptake and hexokinase 2 (HK2), and between glucose uptake and GSH. They also observed two metabolic phenotypes in their cells, both before and after treatment with erlotinib. The authors stated that the maintenance of this phenotype, even with the reduction in glucose uptake, GSH, and HK2 activity after drug treatment, provides avenues for future investigations.

It is exciting to consider the large number of either intra- or extracellular targets that this SCBC device could be used to measure. A difficulty may be in developing simultaneous assays that are compatible with one another, e.g., all assays performed in the same microchamber must use the same binding and wash buffers. However, with the large numbers of cells and analytes that can be measured, ultrahigh levels of information are obtainable, and because it is fabricated in PDMS, the ability to automate and integrate with other cell-based assays should be feasible.

MICROFLUIDIC SYSTEMS FOR INVESTIGATING CELLULAR DYNAMICS

A new and growing area of research is the examination of intracellular pathways in response to dynamic stimulations.³⁸ Cells often respond differently to dynamic inputs as compared to static inputs, and how they respond can allow modifications to existing biological models to make them more accurate. Also, using this approach, one can identify the dominant features in signaling networks or build simple models incorporating only these dominant features. Finally, it is becoming apparent that dynamic signals provide certain advantages in processing when faced with noisy inputs.³⁹ Microfluidic devices, with their unique ability to deliver time-dependent waves of stimulatory solutions, have become an integral part of this research field.⁴⁰

The Takayama, Linderman, and Neubig research groups have been collaborating for several years in the use of dynamic stimulation profiles for the investigation of cellular signaling.^{41,42} To produce pulses of stimulants, a braille display, composed of computer-controlled vertical pins to actuate channels,⁴³ is used to pump from a media-only reservoir or a stimulant reservoir. With this system, square waves of stimulant

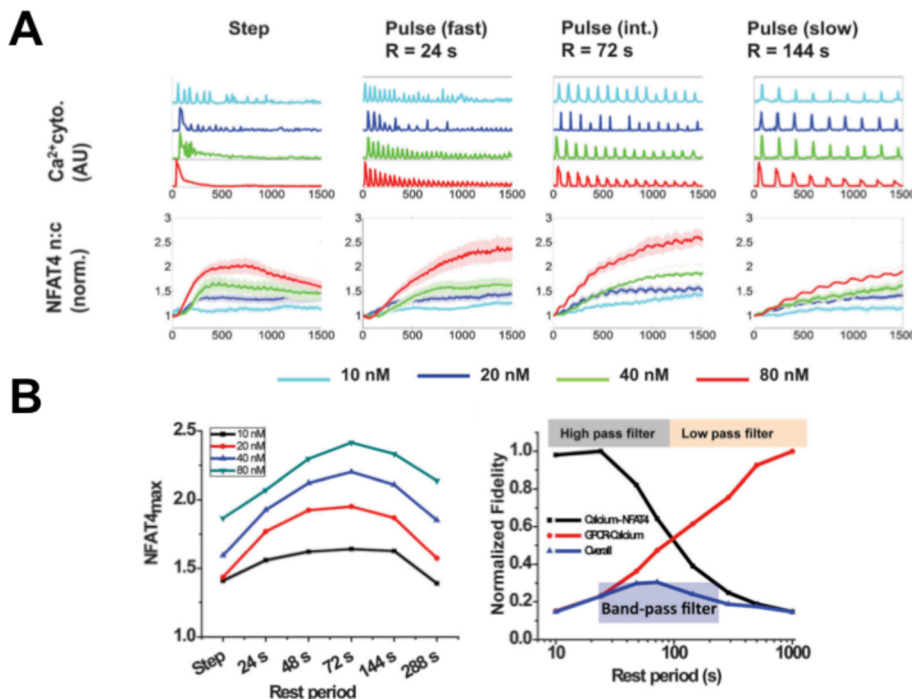


Figure 8. Band-pass processing in GPCR signaling. (A) The dynamics of intracellular Ca^{2+} and NFAT nuclear/cytoplasm (n/c) ratio are shown on the top and bottom rows, respectively, under different carbachol stimulation profiles. The first column shows the results from a step change in carbachol concentration, while the next three columns indicate fast, intermediate, and slow pulses of carbachol where the values of the rest period between pulses were 24, 72, and 144 s, respectively. The carbachol concentration is indicated by the colors shown below the graphs. Slow pulses of carbachol produced the most robust response of Ca^{2+} , whereas intermediate pulses of carbachol produced the largest NFAT n/c ratio. (B) Simulation results showed maximal NFAT4 n/c ratio at intermediate values of the rest period (left panel). The right panel shows the individual components making up the dynamics shown on the left panel. The individual components indicate higher Ca^{2+} fidelity (red line) with long values of the rest period (similar to the data shown in (A)), whereas higher NFAT4 fidelity (black line) with shorter rest periods. Fidelity is the output response normalized to the maximum output. The resulting overall dynamics (blue line) produces the band-pass shape where intermediate values of the rest period produce the highest cellular response. Adapted from Sumit, M.; Neubig, R. R.; Takayama, S.; Linderman, J. J. *Integr. Biol.* 2015, 7, 1378–1386 (ref 44), with permission of The Royal Society of Chemistry.

are delivered to cells and various features of the pulses, such as concentration, duration, and rest period between consecutive stimulations, can be easily controlled.

In a recent paper, they utilized this type of device to investigate the signaling dynamics of a signal transduction pathway composed of a G-protein coupled receptor, the muscarinic M3 receptor, and a transcription factor, nuclear factor of activated T-lymphocytes-4 (NFAT4) in response to the M3 receptor agonist, carbachol.⁴⁴ Considering that the natural analog of carbachol, acetylcholine, can be released in a pulsatile fashion with oscillation periods varying from 0.2 to 6 min,⁴⁵ they set out to understand how such periods might optimize the target cell response. Stimulation with carbachol or acetylcholine results in the release of intracellular Ca^{2+} stores via an inositol trisphosphate-mediated process. The increase of intracellular Ca^{2+} then promotes the translocation of NFAT4 into the nucleus. They utilized transiently transfected Ca^{2+} sensors and GFP-modified NFAT4 in M3 receptor expressing HEK293 cells.

Similar to their previous work,^{41,42} results showed that pulsatile stimulation with carbachol resulted in calcium oscillations that were phase-locked at the specific frequencies of ligand stimulation. However, use of fast ligand pulses (i.e., small rest periods between successive pulses) produced Ca^{2+} oscillations that decayed rapidly over time, whereas Ca^{2+} oscillations elicited by slow ligand pulses were sustained (Figure 8A, top row). They explained this behavior through

the development of a model that incorporated M3 receptor phosphorylation and internalization followed by receptor recycling or degradation. Fast pulses led to less available receptors and a decrease in Ca^{2+} oscillations in time. However, the measured NFAT4 dynamics (nuclear/cytoplasm ratio) was greater for stimulations at intermediate ligand pulse frequencies (Figure 8A, bottom row). How does one rectify these two findings that slow ligand pulses lead to high fidelity calcium responses and intermediate pulses lead to maximum NFAT4 activation?

Using their model and setting M3 receptor desensitization to zero, NFAT4 localization correlated with input ligand frequencies. Therefore, if receptor dynamics were not included, at high ligand frequencies (i.e., short pulses), more NFAT4 was found in the nucleus. However, when receptor desensitization and degradation were added, only low frequency pulses of carbachol were able to elucidate sustained Ca^{2+} pulses. Taken separately, the Ca^{2+} pulsing acts as a low-pass filter whereas the NFAT4 dynamics acts as a high-pass filter. Combining the two systems produces a band-pass where only particular pulse frequencies of carbachol (or presumably acetylcholine) will produce an optimum response of both systems (Figure 8B).

A sensitivity analysis of their model was used to identify both M3 receptor and NFAT4 parameters (e.g., NFAT4 nuclear translocation rate constant) that significantly affected the band-pass characteristics. To showcase how these parameters contribute to the band-pass characteristics, they expanded

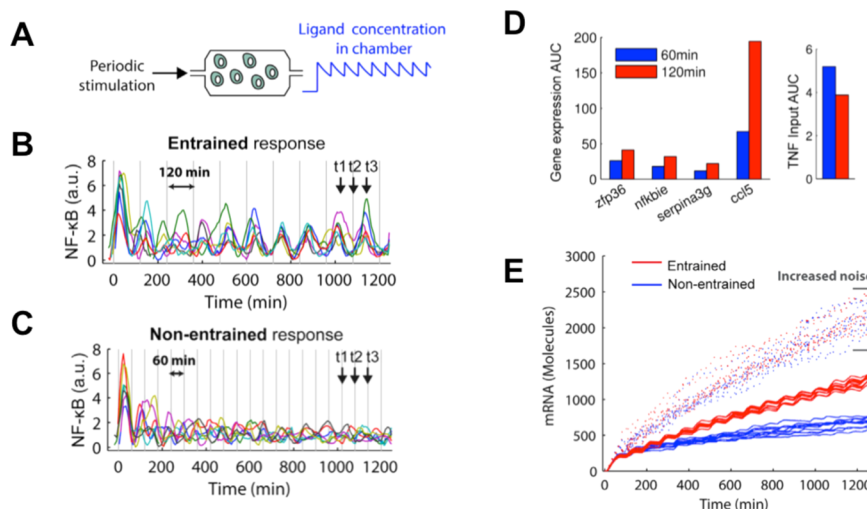


Figure 9. NF- κ B dynamics. (A) Fresh solutions of TNF were delivered to cell chambers producing sawtooth patterns in ligand concentration. (B) Using DsRed-p65, the location of NF- κ B was imaged in single cells (shown by the different colored lines). Application of TNF solutions with 120 min period resulted in an entrained NF- κ B response as observed by the synchronized traces from multiple cells. The vertical, gray lines indicate the period of the TNF delivery. (C) Similar experiment as described in (B), but using a TNF period of 60 min, which resulted in a nonentrained NF- κ B response. (D) Gene expression output from four genes is shown when exposed to 120 min (red) or 60 min (blue) pulses of TNF. Output was quantified using area under the curve (AUC). The total TNF exposure levels for each of the stimulation periods are shown on the right panel, indicating that a 60 min stimulation period had a higher total dosage over the duration of the experiment. (E) Modeling results indicated that the amount of mRNA increased under entrained conditions (red lines) as compared to nonentrained conditions (blue lines) due to cooperative binding of NF- κ B to DNA. Note also the lower variability observed in the mRNA levels for the entrained conditions. The scatter plots show the gene expression levels when the intrinsic noise in their model was increased. Adapted from *Cell*, Vol. 100, Kellogg, R. A.; Tay, S. Noise Facilitates Transcriptional Control under Dynamic Inputs, pp. 381–392 (ref 46). Copyright 2015, with permission from Elsevier.

their study to NFAT1, which has slower nuclear translocation and back-translocation rate constants than NFAT4. The use of NFAT1 resulted in an optimum band-pass that was shifted to lower frequencies. They speculated that band-pass signaling could be involved in a number of other receptor-mediated processes, and depending on the receptor motif, whether slow or fast pulses of ligand would be most efficient (slow pulses for rapid down-regulated receptors; fast pulses for slowly down-regulated receptors).

A paper published in 2015 by Tay's group investigated the effect of oscillatory signaling inputs coupled with intrinsic and extrinsic noise on NF- κ B transcription dynamics.⁴⁶ NF- κ B is a gene regulatory network central to immune function and many diseases. Stimulation with the cytokine, tumor necrosis factor- α (TNF), leads to oscillations in NF- κ B location between the nucleus and cytoplasm with a 90–100 min peak-to-peak interval. How an oscillatory TNF signal impacts NF- κ B signaling is unknown, and how noise, both intrinsic (intracellular variances) and extrinsic (intercell variances), would further attenuate this signaling was investigated using a microfluidics-based experimental pipeline.⁴⁷ This pipeline enabled automated stimulation of 3T3 fibroblasts, live cell imaging of NF- κ B location, and gene expression measurements from 96 independent cell culture experiments each containing ~200 cells.

The PDMS microfluidic device for cell culture and stimulation was based on one that was described in 2007.⁴⁸ For periodic stimulation, TNF was delivered to the cell culture chambers and then incubated for a set period of time, allowing degradation and internalization of the ligand. At defined intervals, the chamber volume was then replaced with fresh TNF leading to a sawtooth pattern in ligand concentration (Figure 9A). NF- κ B subcellular location was interrogated by live cell imaging of DsRed-p65. After stimulation, the cells were

lysed on-chip and the lysate delivered to a 96-well plate where gene expression analysis was performed using a commercial microfluidic system.

The authors found that application of constant TNF to cells resulted in NF- κ B oscillations with a mean period of ~90 min which lasted for more than 24 h. Application of TNF every 120 min, but not 60 min, resulted in NF- κ B oscillations with a similar period as the stimulant, indicating an entrained state (Figure 9B,C). To understand how an entrained versus disorderly NF- κ B dynamic affected gene expression, the expression of target genes was measured with microfluidic qPCR after stimulation with 120 and 60 min periodic TNF pulses. Under the entrained 120 min stimulation, gene expression output was notably enhanced, which was independent of the total TNF dose applied (Figure 9D). A transcriptional model was used to show that this effect was due to nonlinear binding of NF- κ B to DNA. Entrainment also reduced the heterogeneity of single cell gene expression responses (Figure 9E), indicating that entrainment increases both expression output and homogeneity of a cell population. Finally, they demonstrated that, with increased intrinsic noise in their model, gene expression levels were increased.

Why would entrainment and noise result in these outputs? The authors speculated that these features increase the range of periodic inflammatory signals where the cells will respond. In addition, it is likely that oscillatory signals in resonance with the cellular pathway get amplified, whereas those that do not are effectively filtered out. This result may be similar to what was observed in the band-pass signaling of the GPCR pathway,⁴⁴ where particular frequencies would be transmitted, but not others. An important aspect of both of these papers was the modification of cellular models as a result of their experimental observations. This shows the importance of dynamic stimulations in revealing biological aspects that would normally

not be observed under more conventional stimulation protocols.

In a paper published in 2015, the entrainment window of islets of Langerhans was investigated using a microfluidic system.⁴⁹ As mentioned before, islets of Langerhans are mainly composed of pancreatic β -cells that release insulin in response to elevated glucose levels. As glucose enters these cells, metabolism of the sugar results in an increase in intracellular Ca^{2+} and an output of insulin release. The prevailing hypothesis is that, because metabolism of the sugar is oscillatory with a period of 5 min, intracellular Ca^{2+} levels and insulin release are also oscillatory with a period of ~ 5 min.⁵⁰ In vivo, oscillations in blood insulin levels are observed with a similar period, indicating a majority of the $\sim 1,000,000$ islets in the pancreas are synchronized. How these islets synchronize is unknown; yet, oscillatory hormone secretion has been shown to be beneficial to downstream organs such as the liver.⁵¹ One mechanism for how a synchronized response occurs is through entrainment of islets to oscillatory glucose levels in the body.⁵² By measuring the periods of glucose levels that can entrain islets, one can get a better understanding if this mechanism is feasible *in vivo*.

The microfluidic system to examine the entrainment window was relatively simple, composed of two inputs, a mixing channel, and a chamber where a group of ~ 10 islets were held (Figure 10A). The perfusion system used to deliver the glucose to the islets was based on a system reported earlier,⁵³ which consisted of two syringes elevated above the device allowing hydrostatic pressure to drive the solution to the mixing chamber. By controlling the relative height ratio of the two

syringes using a computer-controlled stepper motor, a given concentration of glucose could be delivered. The microfluidic device was placed on an inverted fluorescence microscope for imaging the fluorescence of the Ca^{2+} -sensitive dye, Fura-2, loaded in the islets.

A constant and elevated glucose level was first delivered to induce the natural oscillations of intracellular Ca^{2+} . After a short period of time, a chirped wave of glucose was applied where the amplitude (concentration) of the wave was held constant while the frequency changed linearly in time. The periods of the chirped glucose wave were swept from 20 to 2 min over the experimental time of 60 min while monitoring the intracellular Ca^{2+} within the islets. The average intracellular Ca^{2+} traces from all the islets was then plotted and showed disorganized oscillations during the initial delivery of the constant glucose (Figure 10B). This was due to the islets all oscillating, but being out of phase with one another. Upon application of the chirped wave, the islets continued to oscillate out of phase until a particular range of periods, close to the natural period of the islets, was delivered. When the applied periods were close (approximately within ± 2 min) to the natural periods of the islets, the Ca^{2+} oscillations from the islets synchronized resulting in cohesive population oscillations. By examining individual islet traces, variations in their responses were observed; for example, some islets would respond to large ranges of glucose input periods, and others would not. Also, some islets responded with intracellular Ca^{2+} oscillation periods that were harmonics of the glucose periods. The results indicated that islets show a range of oscillatory periods that resemble those observed *in vivo*, leaving the possibility open that small amplitude glucose oscillations could produce the synchronized insulin pulses observed from the pancreas.

While the measurement of intracellular Ca^{2+} is relatively facile using intracellular fluorescent sensors, it would be more physiologically relevant if insulin levels were measured. To measure the released hormone, this microfluidic perfusion system was also integrated with a separation system in 2015 to measure time-resolved insulin secretion profiles in response to glucose waves.⁵⁴

In a final example of a microfluidic device used to examine cellular dynamics, Lu's group has integrated a deterministic cell trap array⁵⁵ with a perfusion system that delivered waves of H_2O_2 to a large number of cells.⁵⁶ A novel feature of their system was the use of on-chip pneumatic valves in the same plane as the fluidic channels. The authors stated that this design avoided the time-consuming and labor-intensive process of multilayer soft lithography. Most of this paper was devoted to characterizing the fluid dynamics associated with incorporation of this perfusion system with the cell trap array, which was appropriate due to the large number of cells that this array can hold (~ 1000 as shown in ref 55). In the most recent report, they demonstrated entrainment of intracellular Ca^{2+} oscillations from 50 cells to H_2O_2 pulses with a frequency of 5 mHz, but not at 50 mHz, indicating a frequency-dependent response. An exciting feature of this system is the ability to hold a large number of cells and apply complex stimulation profiles, which will allow high throughput characterizations of other non-adherent cell types.

FUTURE OUTLOOKS

The enabling technology of microfluidic systems has sparked a revolution in cellular analysis.⁵⁷ What once was only in the realm of a few analytical laboratories is now available to a wide

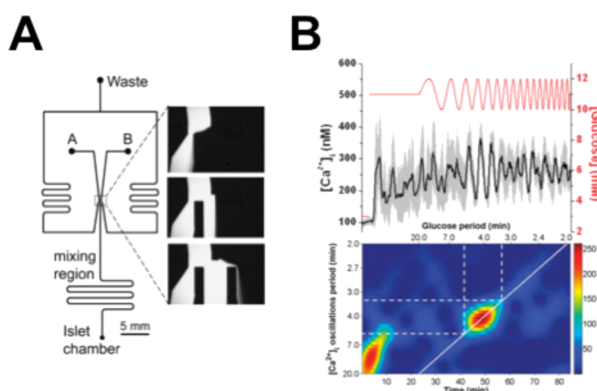


Figure 10. Chirped glucose wave applied to islets of Langerhans. (A) The design of the PDMS microfluidic device is shown which consisted of two inputs (A and B) and two outputs (Waste and Islet chamber). By controlling the relative heights of the two input solutions, different concentrations of glucose (right three images) could be delivered to the Islet chamber, while maintaining a constant total flow rate in the system. (B) The top figure shows the average intracellular Ca^{2+} levels (dark black line) from 7 islets in response to a chirped glucose wave (red line) with periods changing from 20 to 2 min. Error bars on the average Ca^{2+} trace indicate ± 1 standard deviation. Below, the trace is a spectrogram that plots the observed Ca^{2+} oscillation period vs the experimental time (bottom x-axis) or the applied glucose period (top x-axis). The diagonal white line indicates the periods of the glucose wave that were applied to the islets. When periods from 3.4 to 5.4 min were delivered, the Ca^{2+} oscillations from the islets entrained and synchronized, producing the large resonance in the spectrogram. Adapted from Dhumpa, R.; Truong, T. M.; Wang, X.; Roper, M. G. *Integr. Biol.* 2015, 7, 1061–1067 (ref 49), with permission of The Royal Society of Chemistry.

range of researchers and has facilitated novel cellular findings. Microfluidic systems can now be used for analyses of subcellular fractions⁵⁸ to whole organs⁵⁹ or even whole animals.⁶⁰

Future work in this area may be toward the development of new materials that enables production of these devices in a manner that will be economically viable for commercial production. High speed and inexpensive 3D printing is increasing the realm of microfluidics to an even larger audience, so the continued development of these printing systems and materials is valuable.⁶¹ Besides innovations in the microfluidic devices, a driving feature to where we currently are in this field was the development of analytical methods that have the sensitivity necessary for single cell (or smaller) assays. Continued development of quantitative analytical methods in these, and even smaller, volumes will enable even more complex inquiries in the future.

AUTHOR INFORMATION

Corresponding Author

*Phone: 850-644-1846. Fax: 850-644-8281. E-mail: roper@chem.fsu.edu.

Notes

The authors declare no competing financial interest.

Biography

Michael G. Roper is an associate professor in the Department of Chemistry and Biochemistry at Florida State University. He obtained his B.S. in Chemistry at the University of Texas at Austin in 1998 and his Ph.D. from the University of Florida in 2003 and performed postdoctoral work at the University of Virginia from 2003 to 2006. His research interests include the development of high-speed separation methods for measurement of cellular dynamics and the use of microfluidic systems for automating sample preparation.

ACKNOWLEDGMENTS

M.G.R. gratefully acknowledges the help of Mr. Nikita Mukhitov for generating the TOC graphic.

REFERENCES

- (1) Zheng, Y.; Nguyen, J.; Wei, Y.; Sun, Y. *Lab Chip* **2013**, *13*, 2464–2483.
- (2) Kalfe, A.; Telfah, A.; Lambert, J.; Hergenröder, R. *Anal. Chem.* **2015**, *87*, 7402–7410.
- (3) Xu, Y.; Xie, X.; Duan, Y.; Wang, L.; Cheng, Z.; Cheng, J. *Biosens. Bioelectron.* **2016**, *77*, 824–836.
- (4) Charwat, V.; Joksch, M.; Sticker, D.; Purtscher, M.; Rothbauer, M.; Ertl, P. *Analyst* **2014**, *139*, 5271–5282.
- (5) Haandbæk, N.; Bürgel, S. C.; Heer, F.; Hierlemann, A. *Lab Chip* **2014**, *14*, 369–377.
- (6) Waters, L. C.; Jacobson, S. C.; Kroutchinina, N.; Khandurina, J.; Foote, R. S.; Ramsey, J. M. *Anal. Chem.* **1998**, *70*, 158–162.
- (7) Ocvirk, G.; Salimi-Moosavi, H.; Szarka, R. J.; Arriaga, E.; Andersson, P. E.; Smith, R.; Dovichi, N. J.; Harrison, D. J. In *Micro Total Analysis Systems '98*; Springer: Dordrecht, Netherlands, 1998; pp 203–206.
- (8) Schilling, E. A.; Kamholz, A. E.; Yager, P. *Anal. Chem.* **2002**, *74*, 1798–1804.
- (9) Xu, S.; Ainla, A.; Jardemark, K.; Jesorka, A.; Jeffries, G. D. M. *Anal. Chem.* **2015**, *87*, 381–387.
- (10) Ainla, A.; Jeffries, G. D. M.; Brune, R.; Orwar, O.; Jesorka, A. *Lab Chip* **2012**, *12*, 1255–1261.
- (11) Terao, K.; Gel, M.; Okonogi, A.; Fukae, A.; Okitsu, T.; Tada, T.; Suzuki, T.; Nagamatsu, S.; Washizu, M.; Kotera, H. *Sci. Rep.* **2014**, *4*, 4123.
- (12) Gel, M.; Suzuki, S.; Kimura, Y.; Kurosawa, O.; Techamnrat, B.; Oana, H.; Washizu, M. *IEEE Trans. Nanobioscience* **2009**, *8*, 300–305.
- (13) Matharu, Z.; Patel, D.; Gao, Y.; Haque, A.; Zhou, Q.; Revzin, A. *Anal. Chem.* **2014**, *86*, 8865–8872.
- (14) Liu, Y.; Kwa, T.; Revzin, A. *Biomaterials* **2012**, *33*, 7347–7355.
- (15) Hu, J.; Yu, Y.; Brooks, J. C.; Godwin, L. A.; Somasundaram, S.; Torabinejad, F.; Kim, J.; Shannon, C.; Easley, C. J. *J. Am. Chem. Soc.* **2014**, *136*, 8467–8474.
- (16) Zhou, Q.; Kwa, T.; Gao, Y.; Liu, Y.; Rahimian, A.; Revzin, A. *Lab Chip* **2014**, *14*, 276–279.
- (17) Clark, A. M.; Sousa, K. M.; Jennings, C.; MacDougald, O. A.; Kennedy, R. T. *Anal. Chem.* **2009**, *81*, 2350–2356.
- (18) Clark, A. M.; Sousa, K. M.; Chisolm, C. N.; MacDougald, O. A.; Kennedy, R. T. *Anal. Bioanal. Chem.* **2010**, *397*, 2939–2947.
- (19) Dugan, C. E.; Kennedy, R. T. *Methods Enzymol.* **2014**, *538*, 195–209.
- (20) Dugan, C. E.; Cawthorn, W. P.; MacDougald, O. A.; Kennedy, R. T. *Anal. Bioanal. Chem.* **2014**, *406*, 4851–4859.
- (21) Kim, J.; Johnson, M.; Hill, P.; Gale, B. K. *Integr. Biol.* **2009**, *1*, 574–586.
- (22) Kirby, A. E.; Wheeler, A. R. *Anal. Chem.* **2013**, *85*, 6178–6184.
- (23) Shallan, A. I.; Guijt, R. M.; Breadmore, M. C. *Bioanalysis* **2014**, *6*, 1961–1974.
- (24) Hasic, S.; Murthy, S. K.; Koppes, A. N. *Anal. Chem.* **2015**, DOI: [10.1021/acs.analchem.5b04077](https://doi.org/10.1021/acs.analchem.5b04077).
- (25) Hughes, A. J.; Spelke, D. P.; Xu, Z.; Kang, C.-C.; Schaffer, D. V.; Herr, A. E. *Nat. Methods* **2014**, *11*, 749–755.
- (26) Kang, C.-C.; Lin, J.-M. G.; Xu, Z.; Kumar, S.; Herr, A. E. *Anal. Chem.* **2014**, *86*, 10429–10436.
- (27) Waters, K. M.; Liu, T.; Quesenberry, R. D.; Willse, A. R.; Bandyopadhyay, S.; Kathmann, L. E.; Weber, T. J.; Smith, R. D.; Wiley, H. S.; Thrall, B. D. *PLoS One* **2012**, *7*, e34515.
- (28) Cheow, L. F.; Sarkar, A.; Kolitz, S.; Lauffenburger, D.; Han, J. *Anal. Chem.* **2014**, *86*, 7455–7462.
- (29) Wang, Y.-C.; Han, J. *Lab Chip* **2008**, *8*, 392–394.
- (30) Lee, J. H.; Song, Y.-A.; Tannenbaum, S. R.; Han, J. *Anal. Chem.* **2008**, *80*, 3198–3204.
- (31) Wang, Y.-C.; Stevens, A. L.; Han, J. *Anal. Chem.* **2005**, *77*, 4293–4299.
- (32) Salehi-Reyhani, A.; Sharma, S.; Burgin, E.; Barclay, M.; Cass, A.; Neil, M. A. A.; Ces, O.; Willison, K. R.; Klug, D. R. *Lab Chip* **2013**, *13*, 2066–2074.
- (33) Yu, J.; Zhou, J.; Sutherland, A.; Wei, W.; Shin, Y. S.; Xue, M.; Heath, J. R. *Annu. Rev. Anal. Chem.* **2014**, *7*, 275–295.
- (34) Xue, M.; Wei, W.; Su, Y.; Kim, J.; Shin, Y. S.; Mai, W. X.; Nathanson, D. A.; Heath, J. R. *J. Am. Chem. Soc.* **2015**, *137*, 4066–4069.
- (35) Fan, R.; Vermesh, O.; Srivastava, A.; Yen, B. K. H.; Qin, L.; Ahmad, H.; Kwong, G. A.; Liu, C.-C.; Gould, J.; Hood, L.; Heath, J. R. *Nat. Biotechnol.* **2008**, *26*, 1373–1378.
- (36) Shi, Q.; Qin, L.; Wei, W.; Geng, F.; Fan, R.; Shin, Y. S.; Guo, D.; Hood, L.; Mischel, P. S.; Heath, J. R. *Proc. Natl. Acad. Sci. U. S. A.* **2012**, *109*, 419–424.
- (37) Bailey, R. C.; Kwong, G. A.; Radu, C. G.; Witte, O. N.; Heath, J. R. *J. Am. Chem. Soc.* **2007**, *129*, 1959–1967.
- (38) Ang, J.; Ingalls, B.; McMillen, D. *Methods Enzymol.* **2011**, *487*, 279–317.
- (39) Levine, J. H.; Lin, Y.; Elowitz, M. B. *Science* **2013**, *342*, 1193–1200.
- (40) Dhumpa, R.; Roper, M. G. *Anal. Chim. Acta* **2012**, *743*, 9–18.
- (41) Jovic, A.; Howell, B.; Cote, M.; Wade, S. M.; Mehta, K.; Miyawaki, A.; Neubig, R. R.; Linderman, J. J.; Takayama, S. *PLoS Comput. Biol.* **2010**, *6*, e1001040.
- (42) Jovic, A.; Wade, S. M.; Miyawaki, A.; Neubig, R. R.; Linderman, J. J.; Takayama, S. *Mol. BioSyst.* **2011**, *7*, 2238–2244.
- (43) Gu, W.; Zhu, X.; Futai, N.; Cho, B. S.; Takayama, S. *Proc. Natl. Acad. Sci. U. S. A.* **2004**, *101*, 15861–15866.
- (44) Sumit, M.; Neubig, R. R.; Takayama, S.; Linderman, J. J. *Integr. Biol.* **2015**, *7*, 1378–1386.

- (45) Dunant, Y.; Jirounek, P.; Israël, M.; Lesbats, B.; Manaranche, R. *Nature* **1974**, *252*, 485–486.
- (46) Kellogg, R. A.; Tay, S. *Cell* **2015**, *160*, 381–392.
- (47) Kellogg, R. A.; Gómez-Sjöberg, R.; Leyrat, A. A.; Tay, S. *Nat. Protoc.* **2014**, *9*, 1713–1726.
- (48) Gómez-Sjöberg, R.; Leyrat, A. A.; Pirone, D. M.; Chen, C. S.; Quake, S. R. *Anal. Chem.* **2007**, *79*, 8557–8563.
- (49) Dhumpa, R.; Truong, T. M.; Wang, X.; Roper, M. G. *Integr. Biol.* **2015**, *7*, 1061–1067.
- (50) Bertram, R.; Sherman, A.; Satin, L. S. *Am. J. Physiol. Endocrinol. Metab.* **2007**, *293*, E890–E900.
- (51) Matveyenko, A. V.; Liuwantara, D.; Gurlo, T.; Kirakossian, D.; Dalla Man, C.; Cobelli, C.; White, M. F.; Copps, K. D.; Volpi, E.; Fujita, S.; Butler, P. C. *Diabetes* **2012**, *61*, 2269–2279.
- (52) Dhumpa, R.; Truong, T. M.; Wang, X.; Bertram, R.; Roper, M. G. *Biophys. J.* **2014**, *106*, 2275–2282.
- (53) Ferry, M. S.; Razinkov, I. A.; Hasty, J. *Methods Enzymol.* **2011**, *497*, 295–372.
- (54) Yi, L.; Wang, X.; Dhumpa, R.; Schrell, A. M.; Mukhitov, N.; Roper, M. G. *Lab Chip* **2015**, *15*, 823–832.
- (55) Chung, K.; Rivet, C. A.; Kemp, M. L.; Lu, H. *Anal. Chem.* **2011**, *83*, 7044–7052.
- (56) He, L.; Kniss, A.; San-Miguel, A.; Rouse, T.; Kemp, M. L.; Lu, H. *Lab Chip* **2015**, *15*, 1497–1507.
- (57) Duncombe, T. A.; Tentori, A. M.; Herr, A. E. *Nat. Rev. Mol. Cell Biol.* **2015**, *16*, 554–567.
- (58) Liga, A.; Vliegenthart, A. D. B.; Oosthuyzen, W.; Dear, J. W.; Kersaudy-Kerhoas, M. *Lab Chip* **2015**, *15*, 2388–2394.
- (59) Esch, E. W.; Bahinski, A.; Huh, D. *Nat. Rev. Drug Discovery* **2015**, *14*, 248–260.
- (60) Kim, D.; Wu, X.; Young, A. T.; Haynes, C. L. *Acc. Chem. Res.* **2014**, *47*, 1165–1173.
- (61) Gross, B. C.; Erkal, J. L.; Lockwood, S. Y.; Chen, C.; Spence, D. M. *Anal. Chem.* **2014**, *86*, 3240–3253.